International Journal of Heat and Mass Transfer 52 (2009) 3595–3605

Contents lists available at ScienceDirect

International Journal of Heat and Mass Transfer

journal homepage: www.elsevier.com/locate/ijhmt

Estimation for inner surface geometry of furnace wall using inverse process combined with grey prediction model

Chin-Ru Su [a], Cha'o-Kuang Chen [b,*], Wei-Long Liu [c], Hsin-Yi Lai [b]

[a] Department of Mechanical and Computer-Aided Engineering, National Formosa University, Yunlin 632, Taiwan, ROC
[b] Department of Mechanical Engineering, National Cheng Kung University, Tainan 701, Taiwan, ROC
[c] Department of Materials Science and Engineering, National Formosa University, Yunlin 632, Taiwan, ROC

ARTICLE INFO

Article history:
Received 15 December 2008
Received in revised form 12 February 2009
Accepted by 12 February 2009
Available online 22 April 2009

Keywords:
Inverse heat conduction
Virtual area
Reverse matrix
Grey prediction

ABSTRACT

In this work the inner surface geometry of a cylindrical furnace wall is estimated using inverse process method combined with grey prediction model. In estimating process a virtual area extended from the inner surface of furnace wall is used for analysis. The heat conduction equation and the boundary condition are first discretized by finite difference method to form a linear matrix equation; the inverse model is then optimized by linear least-squares error method and the temperatures of virtual boundary are obtained from a few of measured temperatures in furnace wall using the linear inverse model; and finally the temperature distribution of system is got by direct process and the inner surface geometry of furnace wall can be estimated accordingly. The result shows that using inverse process combined with grey prediction model the geometry can be exactly estimated from relatively small number of measured temperatures. Moreover, the effects of measurement error, location, and number of measured points on the estimation for inner surface geometry of furnace wall are discussed in detail.

1. Introduction

In heat conduction problem, if the boundary and initial conditions and the material properties are given, the temperature field of the system can be directly solved. This is the so-called well-posed problem and has the so-called direct solution. If the boundary and initial conditions and the material properties are unknown, but the temperature variations at some specific points in the system are given, the boundary conditions (boundary geometry), initial conditions, and material properties can be inversely estimated. This is the so-called ill-posed problem [1] and has the so-called inverse solution. In inverse heat conduction problem, if the temperatures at some appropriate points on the surface or inside the solid are measured by an infrared optical thermometer or a thermo-couple, the data can then be used to find the initial values and boundary conditions (temperature or boundary geometry) or to analyze some significant parameters, such as thermal conductivity [2,3], surface heat flux [4–6].

The inverse problem of undetermined geometry has been widely used in various industrial applications, for examples, the prediction of geometry of blast furnace inner wall, the prediction of crevice and pitting of furnace wall and the optimization of geometry [7]. If the boundary geometry is unknown, the calculated region cannot be determined due to unknown boundary. Thus, the inverse problem becomes extremely complicated. As for the estimate of undetermined geometry of the boundary by inverse process, a general method was first developed in 1986 by Hsieh and Kassab [8]. This method can also be applied for the estimation of non-linear geometry. A three-dimensional geometry was successfully predicted by the finite element methods proposed by Met et al. [9] and Alexaudrou [10] in 1991. In 1997, Huang and Chao [11] estimated an irregular boundary using a boundary element approach by both conjugate gradient and Levenberg–Marquardt methods. He found that the result obtained by the conjugate gradient method is better than the Levenberg–Marquardt method. The former has many advantages include: (i) needs very short computer time; (ii) does not require a very accurate initial guess for the boundary shape; and (iii) needs less number of sensors. In 1999, Huang and Chen [12] further extended the inverse geometry problem to a multiple region domain for estimating the boundary configurations varied with time and space. This approach can be used as a nondestructive evaluation technique and applied to some problems such as frost thickness estimation in refrigeration system.

Grey theory was pioneered by professor Deng in 1982 [13]. It is especially useful for prediction. Professor Deng considered that most of the existing systems are "generalized energy systems", and emphasized that non-negative smooth discrete functions can be transformed into a series which fits in an appropriate exponential law, the so-called grey exponential law. The key technique for grey prediction is to obtain a new series from an original series

* Corresponding author. Tel.: +886 6 2757575x62140; fax: +886 6 2342081.
E-mail address: ckchen@mail.ncku.edu.tw (C.-K. Chen).

0017-9310/$ - see front matter © 2009 Published by Elsevier Ltd.
doi:10.1016/j.ijheatmasstransfer.2009.02.037

Nomenclature

A	constant matrix constructed from thermal properties and space coordinates
B	coefficient matrix of **C**
Bi	Biot number, $h\bar{r}_o/k$
C	vector constructed from the unknown boundary conditions
D	vector constructed from the boundary conditions
E	product of $\mathbf{A}^{-1}$ and **B**
E, **F**	error function
h	heat transfer coefficient
k	thermal conductivity
R	reverse matrix
$\mathbf{R}_i$	parameter of the deterministic grey dynamic model
$\bar{r}$	dimensional radius of the cylinder
r	dimensionless radius of the cylinder
(r, θ)	cylindrical coordinate
$\mathbf{S}_i$	parameter of the deterministic grey dynamic model
$\overline{T}$	dimensional temperature
T	dimensionless temperature
T	temperature matrix
$T(r, \theta)$	temperature at each grid point (r, θ)
t	time
$U^{(1)}$	input series of the deterministic grey dynamic model
$X^{(0)}$	The initial series
$\hat{X}^{(0)}$	predicted value of $X^{(0)}$
$X^{(1)}$	output series of the deterministic grey dynamic model

Greek symbols

Δr	increment of radial coordinate
$\Delta\theta$	increment of angular coordinate
ω	random number, $-1 < \omega < 1$
σ	measurement errors

Subscripts

est	estimated data
exact	exact temperature
i	index of radial coordinate
j	index of angular coordinate
mea	measured data
m	number of unknown physical quantity
n	number of the linear equations after discretization

using accumulated generating operation (AGO), then to form a differential equation and get its solution from the new series, and finally to obtain the prediction result for the original series by means of inverse accumulated generating operation (IAGO). The grey prediction model GM(1,1) [14] can establish the prediction model with only four continuous data taken from original series. However, its prediction accuracy is much affected by the system properties. In general, the result predicted by GM(1,1) is satisfactory only for the system fitting the grey exponential law. Chen and Tien [15,16] estimated the prediction model parameters using deterministic convergence scheme and proposed a method for prediction, namely, deterministic grey dynamic model (DGDM). There is a transfer function existing between the input and output series for this model, so the prediction accuracy can be largely promoted. In this work, DGDM is combined with the inverse process for estimating the inner surface geometry of a furnace wall in order to reduce the number of really measured points and promote the work efficiency.

2. Physical model and governing equations

Fig. 1 shows a two-dimensional system of cylindrical furnace wall in which $\bar{r}_o$ is the constant outer radius and $\bar{r}_i$ is the inner radius of furnace wall which varies with θ, i.e. $\bar{r}_i = \bar{r}_i(\theta)$ and is the unknown geometry for prediction. For establishing the physical model some assumptions are made as follows.

(1) The system is rigid and unmovable.
(2) The system temperature is stable in long operation period.
(3) There is no heat source and sink inside furnace wall.
(4) The physical properties of furnace wall are homogeneous and isotropic; its thermal conductivity *k* and heat transfer coefficient *h* are taken as constant.
(5) The temperature $\overline{T}_i$ at inner surface of furnace wall, $\bar{r}_i = \bar{r}_i(\theta)$, is constant.

Under these assumptions the temperature $\overline{T}_i$ is relatively high and $\overline{T}_o$ at outer surface of furnace wall is relatively low but still higher than the temperature of surroundings, $\overline{T}_\infty$. Heat should diffuse from inner surface to outer surface and then transfer to surroundings due to $\overline{T}_i > \overline{T}_o > \overline{T}_\infty$. Therefore, the governing equation for the steady two-dimensional system of cylindrical furnace wall can be written as:

$$\frac{\partial^2\overline{T}(\bar{r},\theta)}{\partial\bar{r}^2} + \frac{1}{\bar{r}}\frac{\partial\overline{T}(\bar{r},\theta)}{\partial\bar{r}} + \frac{1}{\bar{r}^2}\frac{\partial^2\overline{T}(\bar{r},\theta)}{\partial\theta^2} = 0 \tag{1}$$

and the accompanying boundary conditions are:

$$\overline{T}(\bar{r},\theta) = \overline{T}_i, \quad \bar{r} = \bar{r}_i \tag{2}$$

$$-k\frac{\partial\overline{T}(\bar{r},\theta)}{\partial\bar{r}} = h(\overline{T}_o - \overline{T}_\infty), \quad \bar{r} = \bar{r}_o \tag{3}$$

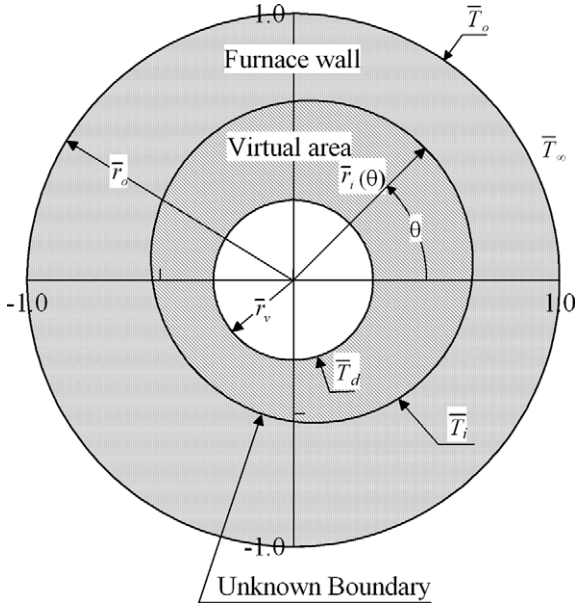

Fig. 1. Two-dimensional system of cylindrical furnace wall with a sinusoidal inner surface containing a virtual area.

The periodic condition in θ direction is

$$\overline{T}(\bar{r},\theta)=\overline{T}(\bar{r},\theta+2\pi) \tag{4}$$

The dimensionless parameters are taken as:

$$r=\frac{\bar{r}}{\bar{r}_o},\quad r_i=\frac{\bar{r}_i}{\bar{r}_o},\quad r_o=\frac{\bar{r}_o}{\bar{r}_o}=1,\quad T=\frac{\overline{T}-\overline{T}_\infty}{\overline{T}_i-\overline{T}_\infty},\quad Bi=\frac{h\bar{r}_o}{k} \tag{5}$$

where Bi is Biot number and $Bi = 2.0$ is used in this work. Eqs. (1)–(4) can be transformed to be dimensionless by putting Eq. (5) into them and written as follows.

$$\frac{\partial^2 T(r,\theta)}{\partial r^2}+\frac{1}{r}\frac{\partial T(r,\theta)}{\partial r}+\frac{1}{r^2}\frac{\partial^2 T(r,\theta)}{\partial \theta^2}=0 \tag{6}$$

$$T(r,\theta)=1,\quad r=r_i \tag{7}$$

$$\frac{\partial T(r,\theta)}{\partial r}=-BiT(r,\theta),\quad r=1 \tag{8}$$

$$T(r,\theta)=T(r,\theta+2\pi) \tag{9}$$

where $T(r,\theta)$ is the temperature at (r,θ) and can be obtained from Eqs. (6)–(9).

In the inverse process for predicting the unknown boundary geometry, $r_i = r_i(\theta)$, a virtual area with an inner boundary, $r = r_v$ and $r_v < r_i(\theta)$, is introduced as shown in Fig. 1. The inner surface of furnace wall has a sinusoidal shape and can be expressed by the following function.

$$r_i(\theta)=0.6+0.1\sin(\theta+45^\circ) \tag{10}$$

There should have a temperature field distributed in the virtual area due to the heat conduction. The temperature field distribution would become steady after a long operation period and the temperature at inner boundary of virtual area should be higher than other boundary. Therefore, the physical model for original system can also be used for the virtual area.

3. Numerical method

3.1. Direct problem

Because the temperature measurement is not performed in practice, the measured temperatures for inverse process are then got from the temperature field of furnace wall obtained by direct process. In direct process for the system shown in Fig. 1, if the three boundary conditions of the furnace wall without virtual area, are given, the governing equation and boundary conditions of Eqs. (6)–(9) can be discretized by finite difference method and written as:

$$\frac{1}{(\Delta r)^2}(T_{i-1,j}-2T_{i,j}+T_{i+1,j})+\frac{1}{r_i}\frac{1}{2\Delta r}(T_{i+1,j}-T_{i-1,j})+\frac{1}{r_i^2}\frac{1}{(\Delta\theta)^2}(T_{i,j-1}-2T_{i,j}+T_{i+1,j})=0 \tag{11}$$

$$T_{i,j}=1,\quad r=r_i \tag{12}$$

$$\frac{T_{I+1,j}-T_{I-1,j}}{2\Delta r}=-BiT_{I,j},\quad r=r_o \tag{13}$$

$$T_{i,o}=T_{i,N} \tag{14}$$

where Δr and $\Delta\theta$ are the increments of dimensionless space coordinates, $T_{i,j}$ is the dimensionless temperature at grid point (i,j), subscript i denotes the ith grid point in r coordinate, subscript j denotes the jth grid point in θ coordinate, subscript I denotes the grid point at outer surface, $r = r_o$, and subscript N denotes the number of grid points in θ direction. Under the case that all boundary conditions are given in direct process, the governing equation of (11) and boundary conditions of (12)–(14) can be rearranged and form a matrix equation:

$$\mathbf{A}_{n\times n}\mathbf{T}_{n\times 1}=\mathbf{D}_{n\times 1} \tag{15}$$

where $\mathbf{A}$ is a constant matrix consisting of thermal properties and space coordinates; $\mathbf{T}$ is a vector consisting of temperature field of discrete points in furnace wall; $\mathbf{D}$ is a vector consisting of the known boundary conditions; and n is the number of discretized linear equations for this system.

If the boundary conditions are known, the temperature field of furnace wall system, i.e. vector $\mathbf{T}$, can be obtained from Eq. (15) by Gauss elimination method in direct process. These temperatures in the temperature field are then taken as the measured temperatures needed in inverse process. For avoiding the actual measurement of temperature inside furnace wall, which needs relatively complicated process and somewhat expensive instruments, a few of temperatures in the temperature field are hence taken as the really measured temperatures, and DGDM is then used to get the indirectly measured temperatures which are taken as the measured temperatures for inverse process.

3.2. The deterministic grey dynamic model

If a system consists of an input series $U^{(0)}(1), U^{(0)}(2), \ldots$ and an output series $X^{(0)}(1), X^{(0)}(2), \ldots$ and the input series can affect the output series through a transfer function, then the system is a dynamic one. Through the transfer function the effect of the input series on the output series at some moment can continue to next several moments. The input series is called leading indicator by economists and the output series is the predicted series. From the research by Box et al. [17], the generalized model for describing continuous dynamic system can be written as:

$$(1+\xi_1 D+\cdots+\xi_p D^p)X(t)=g(1+\eta_1 D+\cdots+\eta_q D^q)U(t) \tag{16}$$

where D denotes d/dt; ξ_p and η_q are constants; U and X are input and output series, respectively. This model is called transfer function model of (p,q) order.

For prediction by grey model GM(1,1), the original series should be treated by AGO. Its aim is to reduce the randomness of series. In this work a prediction method is proposed, which is called deterministic grey dynamic model, simply denotes as DGDM(1,1,1). In this model the grey differential equation GM(p,q) is replaced by Eq. (16), the AGO of GM(p,q) is preserved, and the model parameters are estimated by using deterministic convergence scheme.

Assuming that $U^{(0)}$ and $X^{(0)}$ are input and output series of a dynamic system, and $(U^{(0)}(t),X^{(0)}(t))$ can be obtained by means of observation at equal time intervals, then the DGDM(1,1,1) model can be established by the following steps.

3.2.1. The representation of the transfer function model

For showing the relationship between variations of X and U, a prediction model DGDM(1,1,1) is established by the replacement of the U and X in Eq. (16) by series $U^{(1)}$ and $X^{(1)}$ formed from $U^{(0)}$ and $X^{(0)}$ through 1-AGO, respectively. In DGDM(1,1,1) the first 1 stands for the first-order derivative of 1-AGO series of $X^{(0)}$ series, the second 1 stands for the first-order derivative of 1-AGO series of $U^{(0)}$ series, and the third 1 stands for 1-AGO. Therefore, the grey dynamic model DGDM(1,1,1) can be written as:

$$R\frac{dX^{(1)}(t)}{dt}+X^{(1)}(t)=S_1\frac{dU^{(1)}(t)}{dt}+S_2U^{(1)}(t),\quad t=1,2,\ldots,n \tag{17}$$

where

$$X^{(1)}(t)=\sum_{i=1}^{t}X^{(0)}(i),\quad t=1,2,\ldots,n$$

$$U^{(1)}(t)=\sum_{i=1}^{t}U^{(0)}(i),\quad t=1,2,\ldots,n$$

They are the series formed from $X^{(0)}$ and $U^{(0)}$ by 1-AGO, respectively. R, S_1 and S_2 are the model parameters to be estimated.

3.2.2. The deterministic convergence scheme

The deterministic convergence scheme is one method for estimating the model parameters, in which some kind of error can be reduced to minimum basing on some criterion. To give an example, if the criterion is to minimize the loss function, then it can be written as:

$$E(\beta) = \frac{1}{2}\int_0^T (Y^{(1)} - X^{(1)})'\Omega(Y^{(1)} - X^{(1)})dt \tag{18}$$

where $Y^{(1)} = Y^{(1)}(d,t)$ denotes the real value in process; $X^{(1)} = X^{(1)}(d,t)$ denotes the corresponding model value; and Ω is a weighting matrix. For estimating parameters, the extremum of some function or functional should be obtained. If the criterion is to minimize the error function, i.e.

$$E = E(g_0, g_1, \ldots, g_m) = E(g) \tag{19}$$

where g_i is the model parameters to be determined. The error function defined by Eq. (19) can be regarded as a hypersurface when it is defined as:

$$E(g) = E_0 \tag{20}$$

E_0 is the minimum of the error function, and can be solved by:

$$E_0 = E(g)|_{g=d} \tag{21}$$

The error function can be expanded into a Taylor series at the minimum as follows.

$$E(g) \cong E_0 + \left.\frac{\partial E(g)}{\partial g'}\right|_{g=d}(g-d) + \frac{1}{2}(g-d)'\left.\frac{\partial^2 E(g)}{\partial g \partial g'}\right|_{g=d}(g-d) \tag{22}$$

where E is minimum at $g = d$, $\frac{\partial E(g)}{\partial g'}|_{g=d} = 0$, and $\frac{\partial^2 E(g)}{\partial g \partial g'}|_{g=d}$ is positive definite.

$$\text{Therefore, } E(g) \cong E_0 + \frac{1}{2}(g-d)'\left.\frac{\partial^2 E(g)}{\partial g \partial g'}\right|_{g=d}(g-d) \tag{23}$$

From Eq. (23), the following can be got.

$$\frac{\partial E(g)}{\partial g'} \cong \left.\frac{\partial^2 E(g)}{\partial g \partial g'}\right|_{g=d}(g-d) \tag{24}$$

$$g - d = \left[\left.\frac{\partial^2 E(g)}{\partial g \partial g'}\right|_{g=d}\right]^{-1}\left[\left.\frac{\partial E(g)}{\partial g}\right|_{g=g(t)}\right] \tag{25}$$

Hence,

$$g(i+1) = g(i) - \left[\left.\frac{\partial^2 E(g)}{\partial g \partial g'}\right|_{g=d}\right]^{-1}\left[\left.\frac{\partial E(g)}{\partial g}\right|_{g=g(i)}\right] \tag{26}$$

This is the so-called steepest-descent algorithm.

3.2.3. The evaluation of parameters R, S_1, and S_2

If some process can be described by the following differential equation.

$$\alpha\frac{dY^{(1)}(t)}{dt} + Y^{(1)}(t) = \beta_1\frac{dU^{(1)}(t)}{dt} + \beta_2 U^{(1)}(t), \quad t = 1, 2, \ldots, n \tag{27}$$

and some model can be represented by Eq. (17), then equations of (17) and (27) can be represented by the explicit functions, $X^{(1)}(t) = \ldots$ and $Y^{(1)}(t) = \ldots$, respectively, where $Y^{(1)}(t)$ is the data produced from the really observed values through 1-AGO; $X^{(1)}(t)$ is the data produced from the prediction model values through 1-AGO. Under the case of no interference, the error $e(t) = Y^{(1)}(t) - X^{(1)}(t)$ is small at the optimized state. If $e(t)$ is small enough, then $X^{(1)}(t)$ is nearly equal to

$$\widehat{X}^{(1)}(t) = -RDY^{(1)}(t) + (S_1 D + S_2)U^{(1)}(t) \tag{28}$$

where $D = d/dt$. Therefore,

$$e(t) \cong Y^{(1)}(t) - \widehat{X}^{(1)}(t) \tag{29}$$

$$e(t) \cong (R-\alpha)DY^{(1)}(t) - [(S_1 - \beta_1)D + (S_2 - \beta_2)]U^{(1)}(t) \tag{30}$$

If define

$$R - \alpha = \gamma_1$$
$$S_1 - \beta_1 = \gamma_2$$
$$S_2 - \beta_2 = \gamma_3$$

and

$$DY^{(1)}(t) = v_1(t)$$
$$-DU^{(1)}(t) = v_2(t)$$
$$-U^{(1)}(t) = v_3(t)$$

where v_i, $i = 1, 2, 3$, is obtained by fitting $Y^{(1)}$ and $U^{(1)}$ to a cubic spline curve. Then the following can be obtained:

$$e(t) \cong \sum_{i=1}^{3}\gamma_i v_i$$

$$e^2(t) \cong \sum_{i=1}^{3}\sum_{j=1}^{3}\gamma_i\gamma_j v_i(t)v_j(t)$$

Hence we have

$$E = \int_1^n e^2(t)dt = \sum_{i=1}^{3}\sum_{j=1}^{3}\gamma_i\gamma_j\psi_{ij} \tag{31}$$

where

$$\psi_{ij} = \int_1^n v_i v_j dt = \sum_{t=1}^{n} v_i(t)v_j(t) = \psi_{ji} \tag{32}$$

Eq. (31) can also be written as

$$E = \gamma'\psi\gamma \tag{33}$$

where

$$\gamma' = [\gamma_1, \gamma_2, \gamma_3]$$
$$\psi = \begin{bmatrix} \psi_{11}, & \ldots, & \psi_{13} \\ & \ldots & \\ \psi_{31}, & \ldots, & \psi_{33} \end{bmatrix}$$

Comparison of Eq. (33) with (23) shows that the two equations are equivalent and $E_0 = 0$, hence

$$\left.\frac{\partial^2 E(g)}{\partial g \partial g'}\right|_{g=d} = 2\psi \tag{34}$$

For $\left.\frac{\partial^2 E(g)}{\partial g \partial g'}\right|_{g=d}$ and $\left.\frac{\partial E(g)}{\partial g}\right|_{g=g(i)}$ in Eq. (26), the former is obtained from Eq. (34) and the latter is got by putting Eq. (29) into Eq. (31) and being numerically differentiated. The $\widehat{X}^{(1)}(t)$ in Eq. (29) is the solution of Eq. (17). Eq. (17) can be written as a matrix equation:

$$\mathbf{DG} \cong \mathbf{F} \tag{35}$$

where

$$\mathbf{D}=\begin{bmatrix} -\frac{dX^{(1)(t)}}{dt}|_{t=1}, & \frac{dU^{(1)}(t)}{dt}|_{t=1}, & U^{(1)}(1) \\ -\frac{dX^{(1)}(t)}{dt}|_{t=2}, & \frac{dU^{(1)}(t)}{dt}|_{t=2}, & U^{(1)}(2) \\ \vdots & \vdots & \vdots \\ -\frac{dx^{(1)}(t)}{dt}|_{t=n}, & \frac{dU^{(1)}(t)}{dt}|_{t=n}, & U^{(1)}(n) \end{bmatrix}$$

$$\mathbf{G}=[R,S_1,S_2]^T$$

$$\mathbf{F}=\begin{bmatrix} X^{(1)}(1) \\ X^{(1)}(2) \\ \cdots \\ X^{(1)}(n) \end{bmatrix}$$

And $\mathbf{G}=[R,S_1,S_2]^T$ can be regarded as a correspondent of g in Eq. (26). The solution of least-squares method, $g_0=[R_0,S_{10},S_{20}]^T=(D^TD)^{-1}D^TF$, can be taken as the initial value for the iteration process; and $\frac{dX^{(1)}(t)}{dt}$ and $\frac{dU^{(1)}(t)}{dt}$ can be obtained by fitting $X^{(1)}$ and $U^{(1)}$ to a cubic spline curve.

3.2.4. The application of Fourier series to the fitting of leading indicator

Let

$$\frac{dU^{(1)}(t)}{dt}\cong a_0+\sum_{p=1}^{k}\{a_p\cos[pw(t-1)]+b_p\sin[pw(t-1)]\},\quad t=2,3,\ldots,n+nf \tag{36}$$

Then integrating Eq. (36) gives

$$U^{(1)}(t)\cong U^{(0)}(1)+a_0(t-1)+\sum_{p=1}^{k}\left\{\frac{\sin[pw(t-1)]}{pw}a_p+\frac{1-\cos[pw(t-1)]}{pw}b_p\right\},\quad t=2,3,\ldots,n+nf \tag{37}$$

where w has value of $2\pi/(n+nf)$; k has integral value among $[(n+nf)/2]-1$; nf is the number at prediction time after prediction origin. a_0, a_p, and b_p in Eq. (37) are the parameters to be estimated. If $n+nf$ is taken as an even number, the fitting error of the leading indicator is exactly equal to zero.

3.2.5. The determination of Fourier coefficients

Eq. (37) can be written as

$$B\widehat{A}\cong Y_N \tag{38}$$

where

$$B=\begin{bmatrix} 1, & \frac{\sin w}{w}, & \frac{\sin 2w}{2w}, & \ldots, & \frac{\sin kw}{kw}, & \frac{1-\cos w}{w}, & \frac{1-\cos 2w}{2w}, & \ldots, & \frac{1-\cos kw}{kw}, \\ 2, & \frac{\sin 2w}{w}, & \frac{\sin 4w}{2w}, & \ldots, & \frac{\sin 2kw}{kw}, & \frac{1-\cos 2w}{w}, & \frac{1-\cos 4w}{2w}, & \ldots, & \frac{1-\cos 2kw}{kw}, \\ & & \ldots, & & & & & & \\ & & \ldots & & & & & & \\ z, & \frac{\sin zw}{w}, & \frac{\sin 2zw}{2w}, & \ldots, & \frac{\sin zkw}{kw}, & \frac{1-\cos zw}{w}, & \frac{1-\cos 2zw}{2w}, & \ldots, & \frac{1-\cos zkw}{kw}, \end{bmatrix}$$

$$Y_N=\begin{bmatrix} U^{(1)}(2)-U^{(0)}(1) \\ U^{(1)}(3)-U^{(0)}(1) \\ \cdots \\ U^{(1)}(z+1)-U^{(0)}(1) \end{bmatrix}$$

$$z=n+nf$$

The solution of Eq. (38) obtained by least-squares method is

$$\widehat{A}=[a_0,a_1,\ldots,a_k,b_1,b_2,\ldots,b_k]^T=(B^TB)^{-1}B^TY_N \tag{39}$$

By 1-IAGO to $U^{(1)}$ of Eq. (37), the whitening values can be got as follows.

$$\widehat{U}^{(0)}(1)=U^{(1)}(1)=U^{(0)}(1) \tag{40}$$

$$\widehat{U}^{(0)}(t)=\widehat{U}^{(1)}(t)-\widehat{U}^{(1)}(t-1),\quad t=2,3,\ldots,n+nf \tag{41}$$

3.2.6. The evaluation of $\widehat{X}^{(0)}$

Putting Eqs. (36) and (37) into Eq. (17) obtains

$$\begin{aligned} X^{(1)}(t)=Ae^{-\frac{(t-1)}{R}} &+S_1\left\{a_0+\sum_{p=1}^{k}a_p\frac{\cos[pw(t-1)]+Rpw\sin[pw(t-1)]}{1+R^2p^2w^2}\right. \\ &\left.+\sum_{p=1}^{k}b_p\frac{\sin[pw(t-1)]-Rpw\cos[pw(t-1)]}{1+R^2p^2w^2}\right\} \\ &+S_2\left\{U^{(0)}(1)+a_0(t-1)-Ra_0+\sum_{p=1}^{k}\frac{b_p}{pw}\right. \\ &+\sum_{p=1}^{k}\left[\frac{\frac{1}{pw}\sin(pw\overline{t-1})-R\cos(pw\overline{t-1})}{1+R^2p^2w^2}\right]a_p \\ &\left.-\sum_{p=1}^{k}\left[\frac{R\sin(pw\overline{t-1})+\frac{1}{pw}\cos(pw\overline{t-1})}{1+R^2p^2w^2}\right]b_p\right\} \end{aligned} \tag{42}$$

where A is an arbitrary constant which can be got from the given $X^{(1)}(1)$. By 1-IAGO to $X^{(1)}$ of Eq. (42), the whitening values $\widehat{X}^{(0)}$ can be obtained, which is the prediction values of output series wanted by the present model.

$$\widehat{X}^{(0)}(1)=\widehat{X}^{(1)}(1) \tag{43}$$

$$\widehat{X}^{(0)}(t)=\widehat{X}^{(1)}(t)-\widehat{X}^{(1)}(t-1),\quad t=2,3,\ldots,n+nf \tag{44}$$

To verify the appropriateness for application of DGDM(1,1,1) to the heat conduction problem, as shown in Fig. 2, 10 really measured temperatures at outer surface of furnace wall ($r=1.0$) are taken as

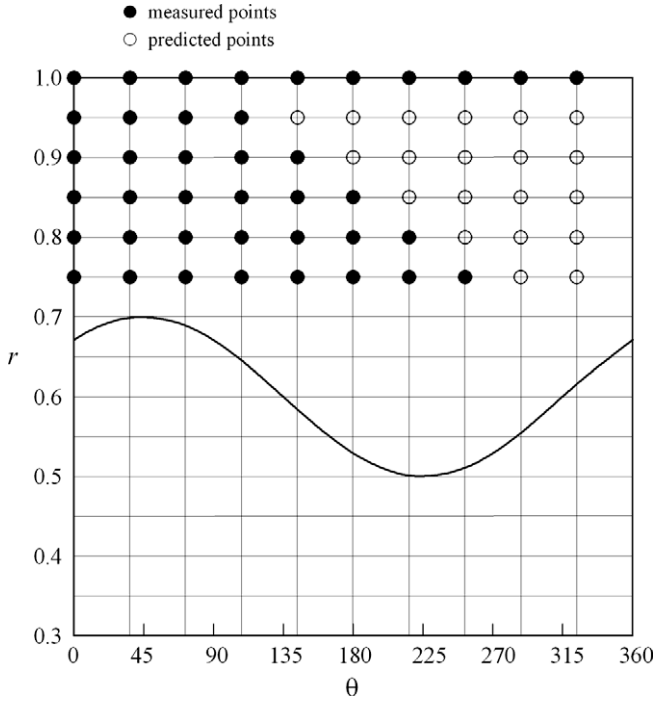

Fig. 2. The schematic diagram for the locations of measured points and predicted points, and the calculated grid of a furnace wall with a sinusoidal inner surface.

Table 1
The results predicted by DGDM(1,1,1) with a input series taken from the temperatures at outer surface of furnace wall ($r = 1.0$) and a prediction series taken from the temperatures at various measured locations under the case without real measurement error, i.e. $\sigma = 0\%$.

Prediction location r	Prediction grid point i	Indirectly measured value $\widehat{X}^{(0)}(i)$	Really measured value $X^{(0)}(i)$	Error percentage of indirect measurement (%)
0.95	5	0.46504	0.46504	0
0.95	6	0.43705	0.43700	0.01
0.95	7	0.43707	0.43700	0.01
0.95	8	0.46506	0.46505	0
0.95	9	0.50919	0.50920	0
0.95	10	0.55992	0.55998	−0.01
0.9	6	0.48091	0.48070	0.04
0.9	7	0.48096	0.48070	0.05
0.9	8	0.51188	0.51183	0.01
0.9	9	0.56057	0.56068	−0.02
0.9	10	0.61649	0.61684	−0.06
0.85	7	0.52766	0.52763	0.01
0.85	8	0.56170	0.56237	−0.12
0.85	9	0.61534	0.61649	−0.19
0.85	10	0.67691	0.67872	−0.27
0.8	8	0.61603	0.61729	−0.20
0.8	9	0.67522	0.67744	−0.33
0.8	10	0.74306	0.74656	−0.47
0.75	9	0.74201	0.74457	−0.34
0.75	10	0.81696	0.82160	−0.56

Table 2
The results predicted by DGDM(1,1,1) with a input series taken from the temperatures at outer surface of furnace wall ($r = 1.0$) and a prediction series taken from the temperatures at various measured locations under the case with a real measurement error, $\sigma = \pm 5\%$.

Prediction location r	Prediction grid point i	Indirectly measured value $\widehat{X}^{(0)}(i)$	Really measured value $X^{(0)}(i)$	Error percentage of indirect measurement (%)
0.95	5	0.52672	0.48752	8.04
0.95	6	0.50453	0.42728	18.08
0.95	7	0.52665	0.43957	19.81
0.95	8	0.56188	0.47277	18.85
0.95	9	0.59546	0.49183	21.07
0.95	10	0.67090	0.55029	21.92
0.9	6	0.50059	0.48785	2.61
0.9	7	0.51058	0.48263	5.79
0.9	8	0.53819	0.49697	8.29
0.9	9	0.56492	0.56954	−0.81
0.9	10	0.64166	0.62239	3.10
0.85	7	0.54708	0.54619	0.16
0.85	8	0.57629	0.54583	5.58
0.85	9	0.60478	0.63006	−4.01
0.85	10	0.68614	0.64483	6.41
0.8	8	0.62124	0.61555	0.92
0.8	9	0.65390	0.66050	−1.00
0.8	10	0.74758	0.71551	4.48
0.75	9	0.73061	0.77187	−5.35
0.75	10	0.83693	0.84623	−1.10

the leading indicator, $U^{(0)}(i)$, $i = 1, 2, ..., 10$, and four really measured temperatures ($r = 0.95$) are taken as the prediction series, $X^{(0)}(i)$, for establishing DGDM(1,1,1). The predicted results are shown in Table 1. Under the case without consideration of measurement error, i.e. $\sigma = 0\%$ the indirectly measured temperatures $\widehat{X}^{(0)}(5) \sim \widehat{X}^{(0)}(10)$ predicated by this model are very consistent with the really measured temperatures. For further understanding the accuracy of the result predicted from various locations by this model, various prediction ways are considered as shown in Fig. 2. The results are shown in Tables 1 and 2, respectively. It can be shown from Table 1 that under the case without real measurement error, $\sigma = 0\%$ the indirectly measured temperatures are very consistent with the really measured temperatures for any prediction location.

Table 2 shows the results for various prediction ways under the case with a real measurement error, $\sigma = \pm 5\%$. It can be shown that the indirect measurement errors are larger than the real measurement errors when six points are predicted by prediction model established from four points data. This phenomenon can be ascribed to the number of predicted data larger than the number of data for establishing model and to the effect of real measurement error, which make the needed information insufficient and the system characteristics vague. When the number of data for establishing model is equal to or larger than the number of predicted data, the accuracy of prediction is still satisfactory even under the case with consideration of real measurement error. It is obvious from the results stated above that the temperatures obtained by DGDM(1,1,1) can be used as the measured temperatures for estimating the inner surface geometry of furnace wall in inverse process.

3.3. Inverse problem

In the inverse process for estimating the inner surface geometry of furnace wall, because the boundary geometry, $r_i(\theta)$, is unknown,

the area for calculation cannot be sure so that the inverse process cannot be performed. Therefore, the concept of virtual area is then introduced in this work. As shown in Fig. 1, a virtual area is added in $r < r_i$ and some assumptions for this virtual area are made as follows. The virtual area has the same thermal conductivity, governing equation, basic assumption, and boundary conditions (except for the inner boundary of virtual area) as the actual system. Therefore, Eq. (12) can be changed as

$$T_{vj} = T_d, \quad r = r_v \tag{45}$$

where $r_v = 0.3$ is used in this work, the subscript v of T_{vj} denotes the grid point at virtual boundary in r direction; T_d is the temperature at grid point (v,j) of virtual boundary.

For performing inverse operation, Eqs. (11), (13), (14), and (45) would be rearranged, and the virtual system can be represented by the following matrix equation.

$$\mathbf{A}_{n\times n}\mathbf{T}_{n\times 1} = \mathbf{B}_{n\times m}\mathbf{C}_{m\times 1} \tag{46}$$

where $\mathbf{A}$ is a constant matrix consisting of thermal properties and space coordinates; $\mathbf{T}$ is a vector consisting of temperatures of measured points; vector $\mathbf{C}$ consists of temperature, $T_{d(v,j)}$, of discrete points for determination; $\mathbf{B}$ is the coefficient matrix of $\mathbf{C}$; n is the number of discretized linear equations; and m is the number of unknown boundary conditions.

It is clear that the linear inverse model formed by matrix equation (46) does not need the assumption of function form for the unknown state and the initially guessed values, which are just the main advantages of reverse matrix method. Putting the measured data into $\mathbf{T}$ in matrix equation, hence the measured value can be represented as $\mathbf{T}_{mea}$.

If the estimated value $\mathbf{C}_{est}$ is given, then $\mathbf{T}_{est}$ can be solved from Eq. (46), i.e.

$$\mathbf{A}\mathbf{T}_{est} = \mathbf{B}\mathbf{C}_{est} \tag{47}$$

The two sides of Eq. (47) are multiplied by $\mathbf{A}^{-1}$, then

$$\mathbf{T}_{est} = \mathbf{A}^{-1}\mathbf{B}\mathbf{C}_{est} = \mathbf{E}\mathbf{C}_{est} \tag{48}$$

where $\mathbf{E} = \mathbf{A}^{-1}\mathbf{B}$.

Comparing estimated value $\mathbf{T}_{est}$ and measured value $\mathbf{T}_{mea}$, their difference can be represented by an error function $\mathbf{F}$.

$$\mathbf{F} = (\mathbf{T}_{est} - \mathbf{T}_{mea})^T(\mathbf{T}_{est} - \mathbf{T}_{mea}) \tag{49}$$

Putting Eq. (48) into Eq. (49) obtains

$$\begin{aligned}\mathbf{F} &= (\mathbf{E}\mathbf{C}_{est} - \mathbf{T}_{mea})^T(\mathbf{E}\mathbf{C}_{est} - \mathbf{T}_{mea}) \\ &= \mathbf{C}_{est}^T\mathbf{E}^T\mathbf{E}\mathbf{C}_{est} - \mathbf{T}_{mea}^T\mathbf{E}\mathbf{C}_{est} - \mathbf{C}_{est}^T\mathbf{E}^T\mathbf{T}_{mea} + \mathbf{T}_{mea}^T\mathbf{T}_{mea}\end{aligned} \tag{50}$$

Differentiating error function $\mathbf{F}$ with respect to $\mathbf{C}_{est}$ and letting it equal to zero, the minimum of $\mathbf{F}$ can be obtained.

$$\frac{\partial \mathbf{F}}{\partial \mathbf{C}_{est}} = 0 \tag{51}$$

Eq. (51) can be solved and simplified, hence

$$\mathbf{E}^T\mathbf{E}\mathbf{C}_{est} = \mathbf{E}^T\mathbf{T}_{mea} \tag{52}$$

Finally the optimum of estimated value $\mathbf{C}_{est}$ can be got by solving following equation.

$$\mathbf{C}_{est} = (\mathbf{E}^T\mathbf{E})^{-1}\mathbf{E}^T\mathbf{T}_{mea} = \mathbf{R}\mathbf{T}_{mea} \tag{53}$$

where $\mathbf{R} = (\mathbf{E}^T\mathbf{E})^{-1}\mathbf{E}^T$ is called the reverse matrix of the unknown boundary conditions.

In sum, if measured value $\mathbf{T}_{mea}$ is given, the optimum of estimated value $\mathbf{C}_{est}$ can be obtained from the reverse matrix. Therefore, the unknown state in inverse problem can be directly solved. This is the so-called linear least-squares error method.

In most experimental methods, the temperatures of discrete points inside furnace wall need not be all measured. In this work only a few measured temperatures are used to solve the temperatures of virtual boundary. A matrix model with reduced dimension can be re-established by only the elements related with measured points, which are parts of the elements in the matrix $\mathbf{R}_{m\times n}$ and vector $\mathbf{T}_{n\times 1}$ of Eq. (53). Therefore, the matrix $\mathbf{R}_{m\times n}$ and vector $\mathbf{T}_{n\times 1}$ are, respectively, reduced as $\mathbf{R}_{m\times n'}$ and $\mathbf{T}_{n'\times 1}$, where $n' < n$ and the number of elements in vector $\mathbf{T}_{n'\times 1}$ is equal to the number of selected measurement points, in other words, the dimension of matrix $\mathbf{R}_{m\times n'}$ may vary with vector $\mathbf{T}_{n'\times 1}$, i.e. the number of measured points would affect the dimension of whole operation matrix. Because Eq. (46) consists of difference equations related to measured temperatures and measured point locations and Eq. (15) consists of equations related to temperature field of whole furnace wall system, the dimension of matrix equation (46) would be much smaller than that of Eq. (15).

The main aim of the present work is to obtain the inner surface geometry of furnace wall. Using governing Eq. (11) and boundary conditions consisting of the outer surface temperature $T_{I,j}$ of furnace wall and the estimated temperature $T_{d(v,j)}$ of virtual boundary obtained from Eq. (53), the temperature field of furnace wall and virtual area can be simply solved by direct process. The isothermal line, $T(r,\theta) = 1$, in temperature field is just the inner surface geometry of furnace wall. It should be noticed that when the isothermal line does not lie on calculated grid points, the exact locations of isothermal line should be calculated by interpolation.

Summing up the matrix relation in direct and inverse problems stated above, Eq. (11) can be re-written, for the arrangement of main elements, as follows.

$$a_iT_{i-1,j} + b_iT_{i,j} + c_iT_{i+1,j} + d_iT_{i,j-1} + e_iT_{i,j+1} = 0 \tag{54}$$

where $a_i \sim e_i$ are constant parameters of space coordinates. Eqs. (13), (14), and (45) can be rearranged and represented as a linear algebraic relation of matrixes.

$$\mathbf{A}\mathbf{T} = \mathbf{B}\mathbf{C} \tag{55}$$

The temperature of virtual boundary, vector $\mathbf{C}$, can be solved using linear least-squares error method in inverse problem.

In Eq. (55)

$$\mathbf{A} = \begin{bmatrix} \overline{\mathbf{A}}_1 & \ddots & \ddots & & \mathbf{O} \\ \ddots & \ddots & c_i\mathbf{I} & \mathbf{O} & \\ \ddots & a_i\mathbf{I} & \overline{\mathbf{A}}_i & c_i\mathbf{I} & \ddots \\ & \mathbf{O} & a_i\mathbf{I} & \ddots & \ddots \\ \mathbf{O} & & \ddots & 2\mathbf{I} & \overline{\mathbf{A}}_I \end{bmatrix}_{(I\cdot J)\times(I\cdot J)}$$

$$\overline{\mathbf{A}}_i = \begin{bmatrix} \ddots & & \ddots & & d_i \\ \ddots & \ddots & \ddots & 0 & \\ \ddots & d_i & b_i & e_i & \ddots \\ & 0 & \ddots & \ddots & \ddots \\ e_i & & \ddots & & \ddots \end{bmatrix}_{J\times J}$$

$$\overline{\mathbf{A}}_I = \begin{bmatrix} \ddots & & \ddots & & d_I \\ \ddots & \ddots & \ddots & 0 & \\ \ddots & d_I & sur & e_I & \ddots \\ & 0 & \ddots & \ddots & \ddots \\ e_I & & \ddots & & \ddots \end{bmatrix}_{J\times J}$$

I is a unit matrix of J order, **O** is zero matrix of J order, $sur = b_I - 2c_I B_i \Delta r$.

$$\mathbf{T} = [\overline{\mathbf{T}}_1 \quad \cdots \quad \overline{\mathbf{T}}_i \quad \cdots \quad \overline{\mathbf{T}}_I]^T$$

$$\overline{\mathbf{T}}_i = [T_{i,1} \quad \cdots \quad T_{i,j} \quad \cdots \quad T_{i,J}]^T$$

$$\mathbf{B} = [\overline{\mathbf{B}}_1 \quad \mathbf{O} \quad \cdots \quad \cdots \quad \mathbf{O}]^T_{J\times(I\cdot J)}$$

$$\overline{\mathbf{B}}_1 = -a_1\mathbf{I}$$

$$\mathbf{C} = [T_{v,1} \quad \cdots \quad T_{v,j} \quad \cdots \quad T_{v,J}]^T$$

The temperatures of virtual boundary obtained from above method and the temperatures of outer surface of furnace wall both can be used to solve the temperature field, vector **T**, of furnace wall and virtual area in direct problem. The linear algebraic relation of matrixes can be changed as

$$\mathbf{AT} = \mathbf{D}$$

where

$$\mathbf{A} = \begin{bmatrix} \overline{\mathbf{A}}_1 & \ddots & \ddots & & \mathbf{O} \\ \ddots & \ddots & c_i\mathbf{I} & \mathbf{O} & \\ \ddots & a_i\mathbf{I} & \overline{\mathbf{A}}_i & c_i\mathbf{I} & \ddots \\ & \mathbf{O} & a_i\mathbf{I} & \ddots & \ddots \\ \mathbf{O} & & \ddots & \ddots & \overline{\mathbf{A}}_{I-1} \end{bmatrix}_{[(I-1)\cdot J]\times[(I-1)\cdot J]}$$

$$\overline{\mathbf{A}}_i = \begin{bmatrix} \ddots & & \ddots & & d_i \\ \ddots & \ddots & \ddots & 0 & \\ \ddots & d_i & b_i & e_i & \ddots \\ & 0 & \ddots & \ddots & \ddots \\ e_i & & \ddots & & \ddots \end{bmatrix}_{J\times J}$$

$$\mathbf{T} = [\overline{\mathbf{T}}_1 \quad \cdots \quad \overline{\mathbf{T}}_i \quad \cdots \quad \overline{\mathbf{T}}_{I-1}]^T$$

$$\overline{\mathbf{T}}_i = [T_{i,1} \quad \cdots \quad T_{i,j} \quad \cdots \quad T_{i,J}]^T$$

$$\mathbf{D} = [\overline{\mathbf{D}}_v \quad \mathbf{O} \quad \cdots \quad \mathbf{O} \quad \overline{\mathbf{D}}_{I-1}]^T$$

$$\overline{\mathbf{D}}_v = -a_1[T_{v,1} \quad \cdots \quad T_{v,j} \quad \cdots \quad T_{v,J}]^T$$

$$\overline{\mathbf{D}}_{I-1} = -c_{I-1}[T_{I,1} \quad \cdots \quad T_{I,j} \quad \cdots \quad T_{I,J}]^T$$

4. Results and discussion

It has been shown in Section 3.2 that the results or the temperatures in furnace calculated by DGDM(1,1,1) is satisfactory. Hence the measured temperatures needed for inverse process can be taken partly from the really measured temperatures and partly from the indirectly measured temperatures obtained from a few of really measured temperatures through DGDM(1,1,1). To verify the appropriateness of the present method, it is necessary to discuss the effect of different numbers of measured points with different locations on the predicted result for the inner surface geometry of furnace wall.

In practice, the temperature measurement always contains some degree of error, of which magnitude depends upon the measuring method employed. Therefore, the simulated temperature measurement adopted in the inverse problem is also considered to include measurement errors. For reasons of practicality, the present study adds a random error noise to the exact temperature values computed from the direct problem. Hence, the measured dimensionless temperature, T_{mea}, is expressed as

$$T_{mea} = T_{exact}(1 + \sigma\omega) \tag{56}$$

where T_{exact} is the field temperature of the measured points obtained from the direct process, ω is a random number between -1 and 1, and σ is the standard deviation of the measurement error.

Fig. 3 shows the temperature field of virtual area and furnace wall with a sinusoidal inner surface, which is obtained from four directly measured temperatures and six indirectly measured temperatures calculated by DGDM(1,1,1) at $r = 0.95$ under the case of neglecting measurement error. The isothermal line, $T(r_i,\theta) = 1$, in Fig. 3 is just the inner surface geometry of furnace wall, which is what the present work wants. Above this isothermal curve is the furnace wall and below is the virtual area. Fig. 4 shows the results

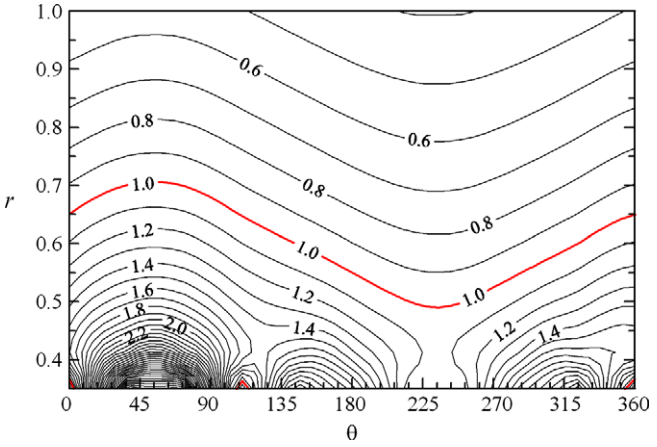

Fig. 3. The temperature field of virtual area and furnace wall with a sinusoidal inner surface, which obtained from four directly measured temperatures and six indirectly measured temperatures calculated by DGDM(1,1,1) at $r = 0.95$ under the case of neglecting measurement error.

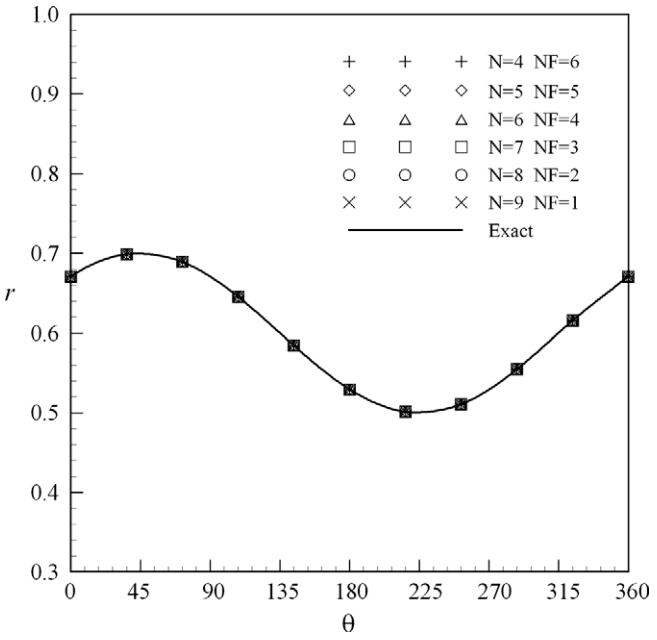

Fig. 4. The inner surface geometry of furnace wall predicted from the temperatures of different measured points and the indirectly measured temperatures calculated by DGDM(1,1,1) at $r = 0.95$ under the case of neglecting the measurement error, i.e. $\sigma = 0\%$. (N, number of measured points; NF, number of predicted points.)

predicted from both temperatures of various measured points and indirectly measured temperatures calculated by DGDM(1,1,1) at $r = 0.95$ under the case without considering measurement error. The indirectly measured temperatures calculated from grey prediction are very consistent with the real temperatures when measurement error is not considered. Therefore, the inner surface geometry can be quite exactly estimated using these temperatures. Under the case with measurement error $\sigma = \pm 5\%$, the estimated result is shown in Fig. 5, the deviation of estimation for the inner surface geometry of furnace wall has an increasing trend due to the number of predicted points calculated by DGDM(1,1,1) not less than really measured points. When the number of predicted points calculated by DGDM(1,1,1) is less than the really measured points, the estimated result is then very consistent with the result (dotted curve) estimated without using DGDM(1,1,1).

For studying the effect of measurement error on the estimation of inner surface geometry of furnace wall, 10 grid points at $r = 0.95$ are selected, which consist of four points calculated by DGDM(1,1,1) and six really measured points, simply denoted DGDM(1,1,1)6–4. The grid points are so selected that the number of really measured points can be decreased and the accuracy of estimation is still preserved. As shown in Fig. 6, the estimated thickness of furnace wall is slightly thinner than the original thickness under the case of $\sigma = +5\%$, which displays the geometry is slightly over estimated. Under the case of $\sigma = -5\%$, the estimated thickness of furnace wall is slightly thicker than the original thickness and this displays the geometry is slightly under estimated. This phenomenon can be ascribed to higher measured values being produced by positive measurement error. In the case that the inner surface temperatures of furnace wall are fixed, only thinner furnace wall can produce higher measured values, and lower measured values are produced by thicker furnace wall. The results are quite consistent with the physical phenomenon. Moreover, in the case of $\sigma = \pm 5\%$ the estimated result has slightly irregular undulation as compared to the exact solution. The estimated results are shown in Fig. 7 for the measurement error of $\sigma = \pm 1\%$, $\pm 2\%$, and $\pm 3\%$, respectively. For the case with measurement error $\sigma = \pm 1\%$, the estimated geometry has a slight deviation from the real values. The estimated values are also increased as measurement error increased to ±2% and ±3%. However, the estimated geometry is still quite exact.

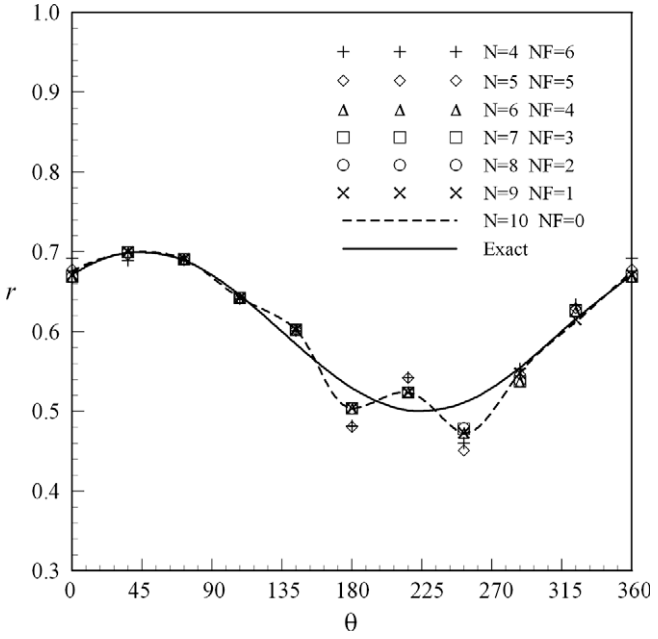

Fig. 5. The inner surface geometry of furnace wall predicted from the temperatures of different measured points and the indirectly measured temperatures calculated by DGDM(1,1,1) at $r = 0.95$ under the case with a measurement error, $\sigma = \pm 5\%$. (N, number of measured points; NF, number of predicted points.)

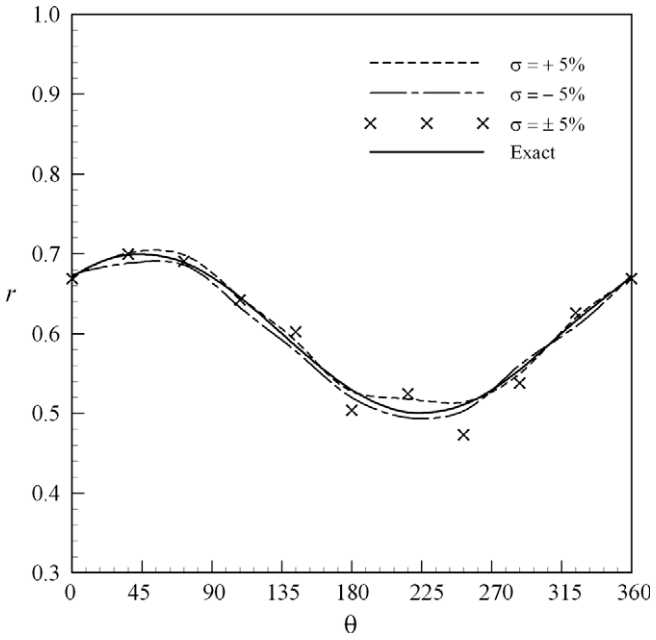

Fig. 6. The effect of measurement error, $\sigma = +5\%$, -5%, and $\pm 5\%$ on the inner surface geometry of furnace wall estimated by DGDM(1,1,1)6–4 from measured points of $r = 0.95$.

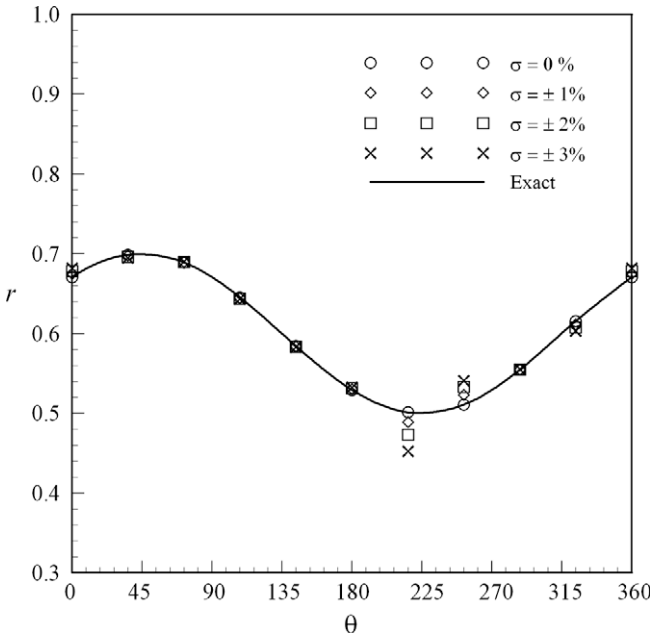

Fig. 7. The effect of measurement error, $\sigma = 0\%$, $\pm 1\%$, $\pm 2\%$, and $\pm 3\%$, on the inner surface geometry of furnace wall estimated by DGDM(1,1,1)6–4 from measured points of $r = 0.95$.

Fig. 8 shows the effect of measured point locations, $r = 0.95$, 0.85, and 0.75, on the estimation of inner surface geometry of furnace wall estimated by DGDM(1,1,1)6–4 for measurement error $\sigma = \pm 5\%$. It can be found that the estimated result is better for the measured points most near inner surface and the estimation deviation would increase with the increase of distance between the measured points and the boundary to be determined. For the

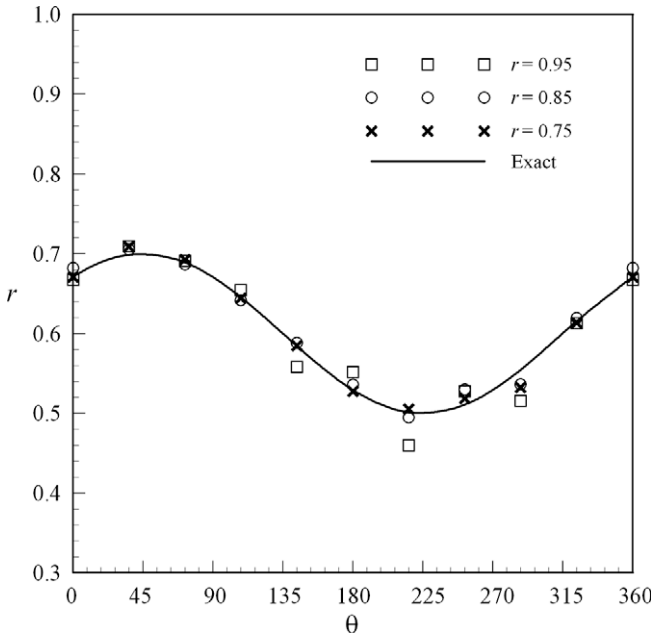

Fig. 8. The effect of measured point location, $r = 0.95$, 0.85, and 0.75, on the inner surface geometry of furnace wall estimated by DGDM(1,1,1)6–4 for measurement error $\sigma = \pm 5\%$.

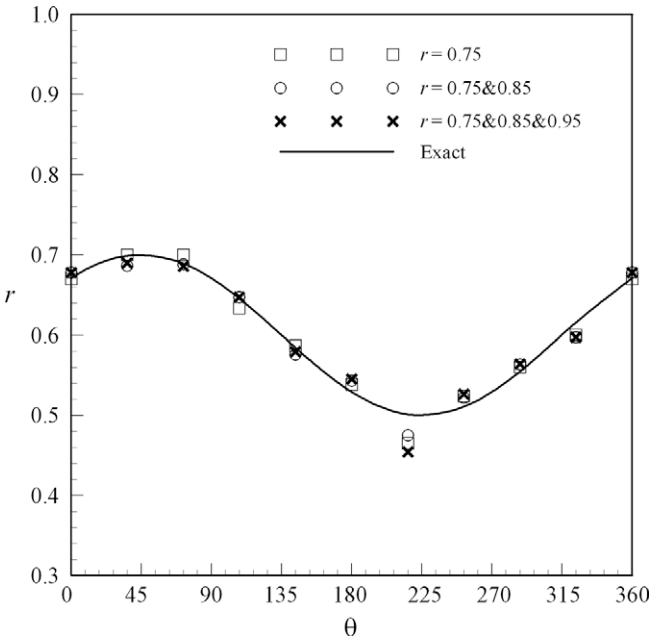

Fig. 10. The effect of measured point number on the inner surface geometry of furnace wall estimated by DGDM(1,1,1)6–4 for measurement error $\sigma = \pm 5\%$.

thicker furnace wall at $135° < \theta < 315°$, the estimation deviation is obviously larger than other thinner furnace wall. These results display that the measured temperatures decrease as the measured points are farther from inner surface, in other words, the measurement error is an important factor for the estimation of inner surface geometry of furnace wall. In any case, the estimated result is still quite precise even for the measured locations much near outer surface.

For studying the effect of measured point number on the estimation of inner surface geometry, the inner surface geometry is first estimated by the values calculated by DGAM(1,1,1)6–4 at $r = 0.95$ for the measurement error $\sigma = \pm 5\%$. The estimated result is shown in Fig. 9. It can be seen that the estimation deviation is relatively large for $135° < \theta < 315°$ due to the farther distance between measured points and boundary, and the other area has quite well estimated result. When a row of measured points are progressively added at $r = 0.85$ and $r = 0.75$, the result is obviously improved for the inner surface far removed from the measured points. Moreover, there is another measurement way as shown in Fig. 10. The measured locations at $r = 0.75$ are first arranged and a satisfactory result can be obtained because these locations are quite near the boundary to be determined. When the number of measured points is increased, i.e. a row of measured points are progressively added at $r = 0.85$ and $r = 0.95$, the accuracy of estimation can be somewhat promoted. In sum, increasing the number of measured points is indeed able to promote the accuracy of estimation.

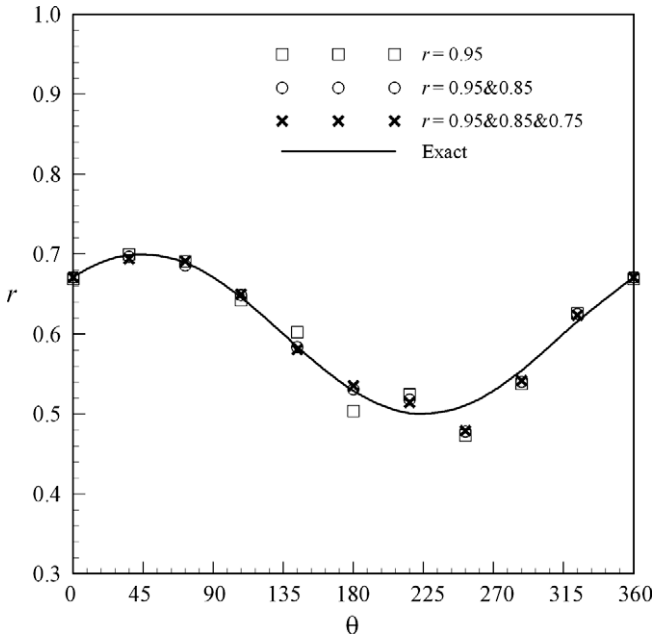

Fig. 9. The effect of measured point number on the inner surface geometry of furnace wall estimated by DGDM(1,1,1)6–4 for measurement error $\sigma = \pm 5\%$.

5. Conclusions

In this work the inverse matrix method combined with DGDM(1,1,1) has been shown that it can be successfully used to estimate the inner surface geometry of furnace wall. It has advantages as follows. The unknown state to be estimated is first represented by a column vector and the estimated values can be obtained by only one operation process in which no assumptions are needed for the function form of unknown state, and the initially guessed values and iteration operation are also not necessary. It is quite efficient for treating unknown conditions with complexity. The accuracy of estimated values is increased with decrease in distance from measured points to the inner surface of furnace wall. In the case with relatively large measurement error, the accuracy of estimated values can be improved by increasing the number of measured points. The estimated values are still accurate even for measurement error of 5%. In inverse process, the accuracy of estimation increases with increase in the number of measured points, and even in the case with a higher measurement error, the accuracy of estimation is still able to be preserved if the number of measured points is sufficient. Although the accuracy of estimation can be increased by the increase of measured points, the measure-

ment cost is then increased and the efficiency is decreased accordingly. Therefore, the DGDM(1,1,1) can be combined to the inverse process to reduce the number of really measured points and still preserve the estimation accuracy. The method proposed in the present work can be applied to the academic and industrial circles.

Acknowledgments

The authors are grateful to the National Science Council of the Republic of China for supporting this research under Grant NSC 97-2221-E-150-071.

References

[1] A.N. Tikhnov, V.Y. Arsenin, Solution of Ill-posed Problems, V.H. Winston, Washington, DC, 1977.
[2] C.Y. Yang, Estimation of the temperature-dependent thermal conductivity in inverse heat conduction problems, Appl. Math. Model. 23 (6) (1999) 469–478.
[3] J.H. Lin, C.K. Chen, Y.T. Yang, Inverse method for estimating thermal conductivity in one-dimensional heat conduction problems, AIAA J. Thermophys. Heat Transfer 15 (1) (2001) 34–41.
[4] P.T. Hsu, Y.T. Yang, C.K. Chen, Simultaneously estimating the initial and boundary conditions in a two-dimensional hollow cylinder, Int. J. Heat Mass Transfer 41 (1) (1998) 219–227.
[5] G.R. Warrier, L.C. Witte, On the application of the hyperbolic heat equation in transient heat flux estimation during flow film boiling, Numer. Heat Transfer A 35 (4) (1999) 343–359.
[6] H.Y. Jang, P.C. Tuan, T.C. Chen, T.S. Chen, Input estimation method combined with the finite-element scheme to solve IHCP hollow-cylinder inverse heat conduction problems, Numer. Heat Transfer A 50 (3) (2006) 263–280.
[7] C.C. Chiang, S.K. Chou, Inverse geometry design problem in optimizing hull surfaces, J. Ship Res. 42 (2) (1998) 79–85.
[8] C.K. Hsieh, A.J. Kassab, A general method for the solution of inverse heat conduction problems with partially unknown system geometries, Int. J. Heat Mass Transfer 29 (1) (1986) 47–58.
[9] L. Met, X.A. Wang, X.Y. Meng, Finite element method to an inverse problem of three-dimensional heat conduction with partially unknown system geometries, in: Proceedings of the International Conference on Numerical Methods in Thermal Problems, 1991, pp. 1514.
[10] A. N. Alexandrou, An inverse finite element method for directly formulated free and moving boundary problems, in: Proceedings of the First International Conference on Computational Modeling of Free and Moving Boundary Problems, 1991, pp. 149–163.
[11] C.H. Huang, B.H. Chao, An inverse geometry problem in identifying irregular boundary configurations, Int. J. Heat Mass Transfer 40 (9) (1997) 2045–2053.
[12] C.H. Huang, H.M. Chen, Inverse geometry problem of identifying growth of boundary shapes in a multiple region domain, Numer. Heat Transfer A 35 (4) (1999) 435–450.
[13] J.L. Deng, Control problems of grey systems, Syst. Control Lett. 1 (5) (1982) 288–294.
[14] J.L. Deng et al., Essential Topics on Grey System: Theory and Applications, China Ocean Press, Beijing, China, 1988.
[15] C.K. Chen, T.L. Tien, A new forecasting method of discrete dynamic system, Appl. Math. Comput. 86 (1) (1997) 61–84.
[16] T.L. Tien, C.K. Chen, The indirect measurement of fatigue limits of structural steel by the deterministic grey dynamic model DGDM(1,1,1), Appl. Math. Model. 21 (10) (1997) 611–619.
[17] G.E.P. Box, G.M. Jenkins, G.C. Reinsel, Time Series Analysis: Forecasting and Control, Prentice-Hall, New Jersey, 1994.